Robust sub-shot-noise measurement via Rabi-Josephson oscillations in bimodal Bose-Einstein condensates

I. Tikhonenkov,[1] M. G. Moore,[2] and A. Vardi[1]
[1]*Department of Chemistry, Ben-Gurion University of the Negev, P.O.B. 653, Beer-Sheva 84105, Israel*
[2]*Department of Physics & Astronomy, Michigan State Univerity, East Lansing, Michigan 48824, USA*
(Received 23 January 2011; published 23 June 2011)

Mach-Zehnder atom interferometry requires hold-time phase squeezing to attain readout accuracy below the standard quantum limit. This increases its sensitivity to phase diffusion, restoring shot-noise scaling of the optimal signal-to-noise ratio in the presence of interactions. The contradiction between the preparations required for readout accuracy and robustness to interactions is removed by monitoring Rabi-Josephson oscillations instead of relative-phase oscillations during signal acquisition. Optimizing the signal-to-noise ratio with a Gaussian squeezed input, we find that hold-time number squeezing satisfies both demands and that sub-shot-noise scaling is retained even for strong interactions.

DOI: 10.1103/PhysRevA.83.063628 PACS number(s): 03.75.Lm, 03.75.Dg, 42.50.Xa

I. INTRODUCTION

Bimodal Bose-Einstein condensates (BECs), realized via double-well confinement [1–4] or internal spin states [5–7], hold great promise for high-precision measurements. Their long phase coherence times and controllability of coupling and interaction parameters make them ideal for the construction of atom interferometers which will make use of quantum correlations to reach unprecedented accuracy.

The current paradigm for matter-wave interferometers is the separated-pulses Mach-Zehnder (MZ) scheme. The bimodal input state is mixed by a 50:50 beam splitter, then held for a fixed duration of relative-phase acquisition in the presence of intermode bias, and then mixed again by a second 50:50 beam splitter. The output number difference then reflects the accumulated phase differential and through it, the bias present during the hold time.

For a two-mode coherent input, the interferometer phase uncertainty $\Delta\theta$ is limited by the standard quantum limit (SQL), $\Delta\theta = 1/\sqrt{N}$, with N being the total number of particles used. The SQL is also known as the "shot-noise limit" because it is essentially the classical expectation for a 50:50 ensemble subject to N measurements. By contrast, the preparation of strongly correlated, number-sqeezed input states can push the phase-estimation uncertainty further down toward the Heisenberg limit $\Delta\theta = 1/N$, which is a factor $\sqrt{N}$ below shot noise [8,9], as demonstrated in two recent experiments [6,7]. In these experiments controlled interactions were used to dynamically generate squeezing via a one-axis twist strategy [10].

While strong interaction is essential for initial number squeezing, it also limits the precision of the interferometer due to phase diffusion during the phase acquisition time [11,12]. To the lowest order, phase diffusion is the shearing of the initial state due to the relative-number-dependent mean-field shift. Hence its rate is proportional to the number variance [11], and the phase squeezing required to attain sub-shot-noise accuracy increases the sensitivity to interactions during the hold time. By contrast, states which are number squeezed during the phase-acquisition period are far more robust but suffer from inherently large readout uncertainty.

One approach to tackle this interplay between readout uncertainty and robustness against phase diffusion is to search for the optimal squeezing and phase-acquisition time which will yield the best accuracy for a given interaction strength and particle number [12–14]. In previous work [13,14], we have carried out such optimization for Gaussian squeezed states (GSSs), which constitute an excellent approximation to the ground state of the bimodal BEC at $T = 0$, with the squeezing controlled by adiabatic variation of the interaction-to-tunneling ratio [15]. The GSS also closely approximates the states formed dynamically by the nonlinear beam splitting of Refs. [6,7]. The noninteracting case was considered in [13] and the effect of interactions was later studied in [14]. In the latter work [14], we adopted the view that the bimodal BEC MZ interferometer measures the "bias," or energy differential ε, between the two wells, rather than the accumulated phase shift $\theta = \varepsilon T$. Thus the hold time T was taken as a free parameter, which can be used in supplement to the initial number-difference variance σ to optimize the signal-to-noise ratio (SNR) $s = \varepsilon/\Delta\varepsilon$ of the interferometer, at any fixed value of N and the dimensionless interaction parameter $\eta = UN/(2\varepsilon)$, where U is the interaction strength.

Using this approach, we found that the optimal preparation changes from a number-squeezed state (transformed to hold-time phase-squeezed state by the beam splitter) with $\sigma_o \sim N^{1/3}$ in the absence of interactions [13] to a phase-squeezed state with $\sigma_o \sim \sqrt{\eta N}$ (here and below o subscripts indicate optimal values) for strong interactions [14]. The resulting optimal SNR is subject to a similar transition from the better than shot noise scaling $s_o \sim N^{2/3}$ without interactions to the strong-interaction behavior of $s_o \sim \sqrt{N/\eta}$. Thus sub-shot-noise precision is lost in the MZ scheme due to interactions and the optimal SNR is worse by a factor $\sqrt{\eta}$ than the standard quantum limit.

Here we consider a different strategy in order to altogether avoid the contradiction between the requirements for readout accuracy (namely hold-time phase squeezing) and robustness to phase diffusion (i.e., hold-time number squeezing). To achieve this goal we replace the roles of the bias ε and hopping K during the signal acquisition stage of the interferometer. Thus, instead of using phase oscillations to monitor ε we

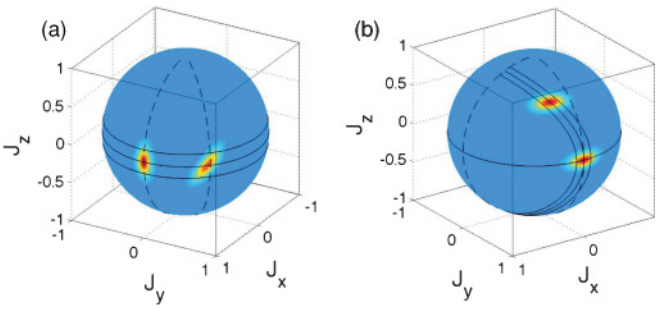

FIG. 1. (Color online) Signal acquisition stage for (a) Mach-Zehnder interferometer and (b) the proposed Rabi-Josephson scheme. Husimi distributions are plotted immediately after the "beam-splitting" and at the end of the hold time. Solid lines depict the classical, mean-field trajectories.

propose to directly measure the nonlinear Rabi-Josephson amplitude oscillation in order to determine K (see Fig. 1). This way, we expect that the preferred preparation for readout accuracy involves hold-time *number* squeezing instead of phase squeezing. Consequently the optimal input states should not lead to faster phase diffusion but in fact be more robust against interactions. Repeating the optimization process, we find that the optimal squeezing scales as $\sigma_o \sim (\tau_o N)^{1/3}$ where $\tau_o = KT_o \sim u^{-1/2}$ and $u = UN/(2K)$ is the pertinent interaction parameter. The optimal acquisition angle τ_o is only residually dependent on N. Consequently, the optimal SNR $s = K/\Delta K$ scales as $s_o \sim (\tau_o N)^{2/3}$. Therefore, stronger phase squeezing $\sigma_o \sim u^{-1/6}$ is preferred for stronger interactions and sub-shot-noise scaling $s_o \sim u^{-1/3}N^{2/3}$ is maintained.

II. EXPERIMENTAL IMPLEMENTATION

Experimentally, double-well potentials are realized by combining a 3D harmonic trap and a 1D optical lattice,

$$V(x,y,z) = \sum_{q=x,y,z} \frac{1}{2} m\omega_q^2 q^2 + V_0 \cos^2(k_0 z), \tag{1}$$

where $\omega_{x,y,z}$ are the trap frequencies along the respective axes and k_0 is the optical lattice wave number. The lattice potential maximum at $z = 0$ splits the bottom of the harmonic trap into a double well. The depth of the optical potential, V_0, then determines the hopping rate, K, of the effective Bose-Josephson Hamiltonian.

A standard Mach-Zehnder interferometer measures the energy imbalance between the two potential minima, which manifests as a J_z rotation. Assuming a perfectly balanced double well in the absence of any additional potentials, the appearance of a nonzero phase shift would therefore indicate the presence of an external field, whose z component could then be deduced from the measured phase shift.

To similarly measure an external applied field via an induced J_x rotation, we propose the following modification to the standard double-well potential:

$$V(x,y,z) = \sum_{q=x,y,z} \frac{1}{2} m\omega_q^2 q^2 + V_0(x) \cos^2(k_0 z); \tag{2}$$

i.e., we make the depth of the optical lattice vary along the x direction. The effect of an external field E_x applied along the x axis would be the shift of the harmonic trap center along x, from $x = 0$ to $x = -E_x/m\omega_x^2$. Typical trap frequencies are ~100 Hz, so that, e.g., a fluctuation in the gravitational acceleration g of one part in 10^4 would shift the trap center by an optical wavelength.

The result of such a shift will be to make the hopping strength dependent on the strength of a field applied along the x axis, $K \to K(E_x)$. A Rabi-Josephson oscillation measurement will reveal K, from which E_x can then be deduced. An interferometer based on the potential (2) would thus be capable of measuring fields along the z axis via a standard relative-phase measurement, as well as measuring fields perpendicular to the z axis via a Rabi-Josephson oscillation amplitude measurement.

III. MEASUREMENT SCHEME AND OPTIMIZATION PROCEDURE

As in previous work, we use the bimodal approximation of the two-site Bose-Hubbard Hamiltonian [16], which accounts for the pertinent physics in current experimental setups [17],

$$H = -K\hat{J}_x + \varepsilon \hat{J}_z + U\hat{J}_z^2. \tag{3}$$

Here K, ε, and U are coupling, bias, and interaction energies, where $U > 0$ corresponds to repulsive interactions and vice versa. The bias ε may be positive or negative, depending on the energy detuning between the two modes. The SU(2) generators $\hat{J}_x = (\hat{a}_1^\dagger \hat{a}_2 + \hat{a}_2^\dagger \hat{a}_1)/2$, $\hat{J}_y = (\hat{a}_1^\dagger \hat{a}_2 - \hat{a}_2^\dagger \hat{a}_1)/(2i)$, and $\hat{J}_z = (\hat{a}_1^\dagger \hat{a}_1 - \hat{a}_2^\dagger \hat{a}_2)/2$, are defined in terms of the boson on-site annihilation and creation operators $\hat{a}_i$, $\hat{a}_i^\dagger$, with the conserved total particle number $n_1 + n_2 = N \equiv 2j$ where $n_i \equiv \hat{a}_i^\dagger \hat{a}_i$.

The standard MZ scheme consists of a fast $\pi/2$ beam-splitter rotation about J_x, followed by relative-phase acquisition during a hold time T due to the bias detuning ε [see Fig. 1(a)], and an opposite $\pi/2$ readout rotation about J_x. The final population imbalance J_z^f is used to read the accumulated phase $\theta = \varepsilon T$ from which the bias ε is readily obtained. Assuming that the beam-splitter and readout rotations are instantaneous with respect to the characteristic phase-diffusion time, the MZ interferometer can be described by the propagator

$$U_{MZI}(\theta,\eta,j) = e^{-i(\pi/2)\hat{J}_x} e^{-i\theta\hat{J}_z[1-(\eta/j)\hat{J}_z]} e^{-i(\pi/2)\hat{J}_x}, \tag{4}$$

where $\eta = Uj/\varepsilon$. The simultaneous operation of phase diffusion and phase acquisition during the hold time T degrades the accuracy of the interferometer, as described in [12,14].

Instead, we propose to employ a Rabi-Josephson (RJ) scheme, summed by the propagator

$$U_{RJ}(\tau,u,j) = e^{-i\tau[\hat{J}_x - (u/j)\hat{J}_z^2]} e^{-i(\pi/2)\hat{J}_z}, \tag{5}$$

where $u = Uj/K$ and $\tau = KT$, in order to determine the value of the coupling strength K from the final population difference. As in our analysis of the MZ interferometer [13,14], this propagator acts on a Gaussian squeezed state, of the form

$$|\sigma\rangle = \frac{1}{\sqrt{\mathcal{N}_\sigma}} \sum_{m=-j}^{j} \exp\left[-\frac{m^2}{4\sigma^2}\right] |j,m\rangle, \tag{6}$$

where σ is the initial number-difference uncertainty, and $\mathcal{N}_\sigma = \sum_{m=-j}^{j} \exp[-m^2/(2\sigma^2)] \approx \sqrt{2\pi}\sigma$. Such states approximate

well the ground state of Hamiltonian (3) with $U > 0$ and $\varepsilon \approx 0$ [15], as well as the dynamically squeezed preparations observed in recent experiments [6,7,10]. As illustrated in Fig. 1(b), the first fast $\pi/2$ rotation about J_z brings the center of the GSS onto the J_y axis, thus allowing for large amplitude Rabi oscillations about J_x during the hold time. The scheme is somewhat reminiscent of a previously proposed Rabi interferometer designed to measure the Casimir-Polder force [18]. However, while the goal in [18] is to determine ε via the detuned Rabi frequency $\sqrt{K^2+\varepsilon^2}$, thus requiring both hopping and detuning to be turned on during the hold time, here we aim to determine K, assuming $\varepsilon = 0$ throughout the acquisition stage. Also in contrast to Ref. [18], which considers only technical experimental noise, here we focus on the sensitivity to collision-induced phase diffusion.

In contrast to the MZ interferometer, where the commutation of the operators for phase acquisition and phase diffusion allows for separation of the two processes and the derivation of analytic expressions, we now have to carry out the simultaneous evolution under $\hat{J}_x$ and $\hat{J}_z^2$. This amounts to the nonlinear mean-field Bose-Josephson oscillation, accompanied by the deformation of the initial distribution due to the variation of initial conditions. We evaluate the final population difference $J_z^f = \langle \hat{J}_z \rangle_T$ and its variance $(\Delta J_z^f)^2 = \langle \hat{J}_z^2 \rangle_T - \langle \hat{J}_z \rangle_T^2$. Using the error propagation estimate $\Delta K = \Delta J_z^f / (\partial J_z^f / \partial K)$, we find that the SNR ratio is given by

$$s = \frac{K}{\Delta K} = \left| \frac{\partial J_z^f}{\partial \tau} \right| \frac{\tau}{\Delta J_z^f}. \tag{7}$$

This quantity is optimized with respect to the parameters $\{\sigma,\tau\}$ in order to obtain the maximum signal-to-noise ratio. Because the final state $|\sigma,\tau\rangle \equiv U_{RJ}|\sigma\rangle$ depends only on the parameters $\{\tau,u,j,\sigma\}$, it follows that the optimal values (σ_o,τ_o) that give the maximum SNR, $s_o = s(\sigma_o,\tau_o)$, as well as s_o itself, are functions of the particle number $N = 2j$ and the interaction-to-tunneling ratio u only. Our goal is to determine the scaling of s_o with j and u and to establish whether sub-shot-noise scaling of s_o is maintained in the presence of interactions.

IV. NUMERICAL OPTIMIZATION RESULTS

Using direct numerical diagonalization, we have simulated the dynamical evolution of the initial state (6) under the propagators (4) and (5), extracting the pertinent signal-to-noise ratios and optimizing them with respect to the initial number variance σ and the hold time T. In Fig. 2 we plot the results of such numerical evaluation (solid lines) of the optimal squeezing σ_o required to obtain the best SNR in both the MZ [Figs. 2(a) and 2(c)] and RJ [Figs. 2(b) and 2(d)] schemes, as a function of the pertinent interaction parameters (η for MZ or u for RJ) and particle number j. Symbols correspond to the analysis outlined below in Sect. V. For both MZ and RJ schemes, the optimal squeezing, as well as the resulting SNR (Fig. 4), coincide in the weak-interaction regime $\eta,u < 1/2$, with the previously studied interaction-free MZ propagation [13]. This is expected because without interaction the choice of axes is immaterial and the RJ sequence may be viewed as a simple rotation of the standard MZ interferometer.

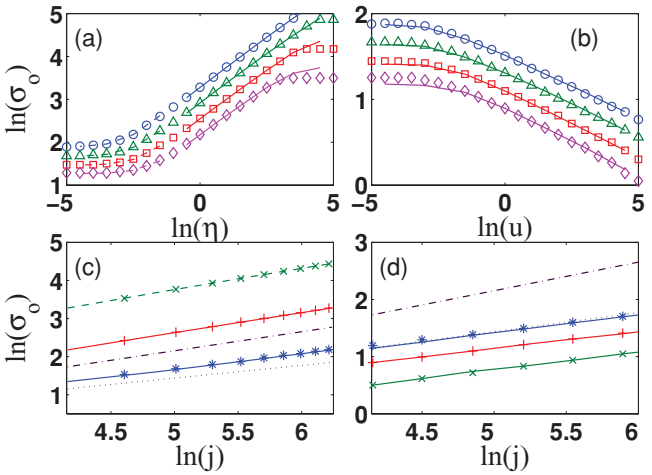

FIG. 2. (Color online) Optimal initial number variance σ_o required to maximize the SNR: (a) as a function of interaction strength η at fixed $j = 64$ ($\diamond$), 128 ($\square$), 256 ($\triangle$), and 512 ($\circ$) for a MZ interferometer; (b) same for the proposed RJ scheme, with u being the relevant hold-time interaction parameter; (c) as a function of the atom number j at fixed interaction strength $\ln(\eta) = -2.5$ ($*$), 0 ($+$), and $+2.5$ ($\times$) for the MZ interferometer; (d) same for RJ scheme with same values of $\ln(u)$ using the same notation convention. Symbols in all panels denote full numerical simulation results. Lines in (a), (c) correspond to analytic expressions obtained in Ref. [14] for weak interaction (dashed) and strong interaction (solid). Solid lines in (b), (d) correspond to the BBR truncated cumulant expansion [20]. Dotted lines in panels (c), (d) mark the interaction-free optimal-squeezing scaling $\sigma_o = j^{1/3}$ whereas dash-dotted lines mark the coherent-state (classical) variance $\sigma = \sqrt{j}$.

For stronger $\eta,u > 1/2$ interactions (corresponding to the Josephson regime [19] for the RJ scheme), however, significant differences are observed.

For the MZ sequence, the optimal initial number variance increases with increasing interactions, until a transition from optimal initial number squeezing ($\sigma_o < \sqrt{j/2}$) to optimal initial phase squeezing ($\sigma_o > \sqrt{j/2}$) takes place as η crosses unity. This transition results from the said contradiction between projection noise minimization (initial number squeezing, hold-time phase squeezing) and phase-diffusion control (initial phase squeezing, hold-time number squeezing). Thus, while for weak interaction ($\eta \ll 1$), we obtain sub-Poissonian scaling $\sigma_o \propto j^{1/3}$ [13], in the presence of strong interactions ($\eta > 1$) we have super-Poissonian optimal-input number distribution with $\sigma_o \propto \sqrt{\eta N}$ [14]. In comparison, the optimal squeezing in the RJ scheme does not follow a similar compromise. Initial number squeezing is preferred for both weak and strong interactions, and in fact becomes stronger with increasing the value of the interaction strength u. The optimal squeezing in this case is found numerically to scale as $(\tau_o N)^{1/3}$.

Significant differences between the standard and proposed schemes also appear in the behavior of the optimal acquired angle ($\theta_o = \varepsilon t_o$ for MZ and $\tau_o = K t_o$ for RJ), shown in Fig. 3. For negligible interactions, both are optimized by $\sim 3\pi/8$ [14] as the pure Rabi oscillation is a simple rotation of the phase-oscillations of the Mach-Zehnder interferometer. However, the j dependence of the optimal τ in the RJ scheme

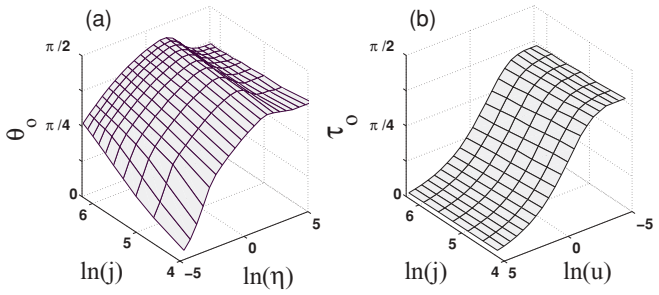

FIG. 3. Optimal acquired angle $\theta_o = \varepsilon T_o$, $\tau_o = KT_o$ required to maximize the SNR for (a) the MZ and (b) the RJ schemes, respectively, as a function of the pertinent interaction parameter η,u and the particle number j.

in the presence of interactions is much weaker than that of θ_o for the MZ interferometer. The resulting maximized precision $p_o = \ln_{10} s_o$ (p_o corresponds to the number of significant readout figures) is plotted in Fig. 4, using the same conventions and ordering. For the MZ scheme, the weak-interaction sub-shot-noise scaling $s_o \propto j^{2/3}$ [13] is replaced by $s_o \propto \sqrt{N/\eta}$ for $\eta > 1$, i.e., worse than the standard quantum limit. The RJ scheme is far more robust to interaction and the SNR deterioration is slower than $s_o \propto u^{-1/3}$ as compared to $s_o \propto u^{-1/2}$ for the MZ scheme [14]. Consequently, the RJ scheme *retains sub-shot-noise scaling*, with $s_o \sim (\tau_o N)^{2/3}$.

V. BOGOLIUBOV ANALYSIS

For the MZ scheme we were able to derive exact analytic expressions for the dynamics with general Gaussian initial conditions and extract the pertinent scaling laws for σ_o and s_o by retaining leading order terms in the various interaction regimes [12,14]. Such derivation is not possible for the proposed RJ

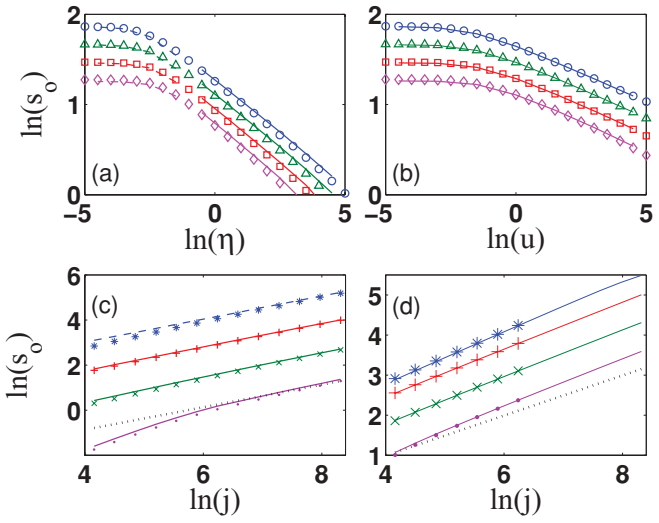

FIG. 4. (Color online) Optimal precision $p_o \equiv \ln s_o$. Panels are arranged in the same order as in Fig. 2. Values of j in panels (a), (b) are also the same. In (c) and (d), the values of $\ln(\eta)$ and $\ln(u)$, respectively, are -2.5 ($*$), 0 ($+$), 2.5 ($\times$), and 5 ($\cdot$). Using the same notation as in Fig. 2, markers denote numerics, whereas lines are analytic estimates (a), (c) and BBR approximate values (b), (d). Dotted lines in (c), (d) mark shot-noise scaling $s \sim j^{1/2}$.

scheme due to the incommutability of the $\hat{J}_x$ and $\hat{J}_z^2$ terms during the acquisition stage. In order to analytically prove the numerically observed scaling relations of the RJ scheme, we employ a density-matrix cumulant-expansion technique developed under the name Bogoliubov back-reaction (BBR) [20]. The hierarchy of dynamical equations for the $\hat{J}_i$ operators is truncated at second order to obtain equations of motion for the mean-field single-particle Bloch vector $\mathbf{R} \equiv \langle \hat{\mathbf{J}} \rangle / j$ and the correlation functions $\Delta_{ij} = (\langle \hat{J}_i \hat{J}_j + \hat{J}_j \hat{J}_i \rangle - 2\langle \hat{J}_i \rangle \langle \hat{J}_j \rangle)/j^2$. Neglecting the back-action terms, these read

$$\begin{aligned}
\dot{R}_x &= -2uR_yR_z, \\
\dot{R}_y &= s_z + 2uR_xR_z, \\
\dot{R}_z &= -R_y \\
\dot{\Delta}_{xx} &= -4u(R_y\Delta_{xz} + R_z\Delta_{xy}), \\
\dot{\Delta}_{yy} &= 2\Delta_{yz} + 4u(R_x\Delta_{yz} + R_z\Delta_{xy}), \\
\dot{\Delta}_{zz} &= -2\Delta_{yz}, \\
\dot{\Delta}_{xy} &= \Delta_{xz} + 2uR_z(\Delta_{xx} - \Delta_{yy}) + 2u(R_x\Delta_{xz} - R_y\Delta_{yz}), \\
\dot{\Delta}_{xz} &= -\Delta_{xy} + 2u(R_y\Delta_{zz} + R_z\Delta_{yz}), \\
\dot{\Delta}_{yz} &= \Delta_{zz} - \Delta_{yy} + 2u(R_x\Delta_{zz} + R_z\Delta_{xz}),
\end{aligned} \tag{8}$$

where $\dot{f} \equiv df/d\tau$.

Given the values of $\mathbf{R}$ and Δ_{ij} after the preliminary $\pi/2$ rotation about J_z,

$$\mathbf{R}_0 = (0,1,0),\ \Delta_{xy,0} = \Delta_{xz,0} = \Delta_{yz,0} = 0,$$

$$\Delta_{xx,0} \approx \frac{1}{2\sigma^2},\ \Delta_{yy,0} \approx \frac{1}{16\sigma^4},\ \Delta_{zz,0} \approx \frac{2\sigma^2}{j^2}, \tag{9}$$

we obtain an exact solution to Eqs. (8) in terms of elliptical Jacobi functions (see Appendix). To leading order, we find that

$$(\Delta J_z^f)^2/j^2 = \Delta_{zz}(\tau)/2 \approx \frac{u^2\tau^6}{36\sigma^2} + \frac{\tau^2}{32\sigma^4} + \frac{\sigma^2}{j^2}, \tag{10}$$

$$\frac{1}{j}\left|\frac{\partial J_z^f}{\partial \tau}\right| = |R_y(\tau)| \approx \sqrt{1 - \tau^2 - u^2\tau^4}. \tag{11}$$

Substituting into Eq. (7) and focusing on the strong-interaction regime $u\tau \gg 1$, we obtain

$$s^2(\tau,\sigma) = \frac{\tau^2(1 - u^2\tau^4)}{\frac{u^2\tau^6}{36\sigma^2} + \frac{\tau^2}{32\sigma^4} + \frac{\sigma^2}{j^2}}. \tag{12}$$

Optimizing $s(\tau,\sigma)$ with respect to τ and σ results in

$$u^2\tau^4\sigma^2 = A(u,\tau),\ \sigma^2 = B(u,\tau)j^{2/3}\tau^{2/3}, \tag{13}$$

where the functions

$$A(u,\tau) = \frac{9}{4}\frac{1 - 4u^2\tau^4}{1 + 3u^2\tau^4},\ B(u,\tau) = \left(\frac{1}{16} + \frac{A(u,\tau)}{36}\right)^{1/3}$$

only depend weakly on u and τ and could therefore be assumed constant. Thus we conclude that the scaling of the optimal initial number variance σ_o and hold time τ_o required to obtain the best SNR s in the RJ scheme is

$$\sigma_o^2 = (j\tau_o)^{2/3}/2, u^2\tau_o^4\sigma_o^2 = 9/4. \tag{14}$$

This is consistent with the numerically obtained $\sigma_o \sim u^{-1/6}j^{1/3}$, $s_o \sim j^{2/3}u^{-1/3}$ scaling in Figs. 2 and 4. The results

of the BBR optimization are shown as symbols in Figs. 2(b) and 2(d) and Figs. 4(b) and 4(d), and agree well with the numerics.

VI. CONCLUSIONS

Due to their strong interaction, phase diffusion is an eminent obstacle to the realization of sub-shot-noise interferometry in dilute quantum gases. The standard Mach-Zehnder scheme, borrowed from linear optical interferometry, suffers from an inherent contradiction between the preparation of a number-squeezed input state required for sub-shot-noise precision and its increased sensitivity to interactions during the signal acquisition time after it has been converted to a phase-squeezed state by the beam splitter [12,14]. Placing the measured perturbation between the sites so that it affects the odd-even detuning instead of the bias between sites, and monitoring Rabi-Josephson amplitude oscillations instead of phase oscillations, removes this contradiction. We have shown that number-squeezed states satisfy both readout and robustness requirements and that, in fact, increased number squeezing optimizes the input states in the presence of interactions. This is distinct from the MZ scheme, where a transition occurs from optimal hold-time phase squeezing (optimizing readout) to optimal number squeezing (optimizing robustness) as the interactions cross a critical magnitude [14]. As a result, the best SNR ratio obtained by the RJ scheme retains sub-shot-noise scaling, as opposed to the super-shot-noise scaling of the SNR of a MZ interacting atom interferometer.

ACKNOWLEDGMENTS

This work was supported by the Israel Science Foundation (Grant No. 582/07), by Grant No. 2008141 from the United States–Israel Binational Science Foundation (BSF), and by the National Science Foundation through a grant for the Institute for Theoretical Atomic, Molecular, and Optical Physics at Harvard University and Smithsonian Astrophysical Observatory.

APPENDIX : SOLUTION OF THE BBR EQUATIONS

Given the set of equations (8) with the initial conditions (9), an exact analytic solution for the mean-field equations for **R** is found in the form of Jacobian elliptic functions,

$$\begin{aligned} R_x &= uR_z^2, \\ R_y &= \sqrt{1-R_z^2-u^2R_z^4}, \\ R_z &= -R_m \mathrm{cn}(\tau(1+4u^2)^{1/4}-K(k)), \end{aligned} \tag{A1}$$

where $R_m^2 = 2/(1+\sqrt{1+4u^2})$, $k^2 = (1-1/\sqrt{1+4u^2})/2$, $K(k) = \int_0^{\pi/2} d\phi (1-k^2\sin^2\phi)^{-1/2}$ is the quarter period, and

$$\tau = \int_0^{|R_z|} \frac{d\zeta}{\sqrt{1-\zeta^2-u^2\zeta^4}}.$$

The equations for the fluctuations Δ_{ij} may then be solved in the form

$$\begin{pmatrix} \Delta_{xx} & \Delta_{xy} & \Delta_{xz} \\ \Delta_{xy} & \Delta_{yy} & \Delta_{yz} \\ \Delta_{xz} & \Delta_{yz} & \Delta_{zz} \end{pmatrix} = C^T \begin{pmatrix} \Delta_{xx,0} & 0 & 0 \\ 0 & \Delta_{yy,0} & 0 \\ 0 & 0 & \Delta_{zz,0} \end{pmatrix} C, \tag{A2}$$

where the elements c_{ij} of the orthogonal matrix C satisfy

$$\begin{aligned} \dot{c}_{1a} &= -2uR_z c_{2a} - 2uR_y c_{3a}, \\ \dot{c}_{2a} &= (1+2uR_x)c_{3a} + 2uR_z c_{1a}, \\ \dot{c}_{3a} &= -c_{2a}, \end{aligned} \tag{A3}$$

with initial values $c_{ab}(t=0) = \delta_{ab}$ and $a,b = 1,2,3$. Parametrizing the solutions in terms of the variable $\rho = -R_z$ and noting that

$$\frac{dc_{ab}}{d\tau} = \frac{dc_{ab}}{d\rho}\sqrt{1-\rho^2-u^2\rho^4}, \tag{A4}$$

we find the following series expansions:

$$\begin{aligned} c_{11} &= 1 - 2u\sum_{n=1}^{\infty}\alpha_n\rho^{2n+2}, \\ c_{21} &= -\sqrt{1-\rho^2-u^2\rho^4}\sum_{n=1}^{\infty}(2n+1)\alpha_n\rho^{2n+1}, \\ c_{31} &= \sum_{n=1}^{\infty}\alpha_n\rho^{2n+1}, \\ c_{12} &= 2u\sum_{n=0}^{\infty}\frac{\beta_n}{2n+1}\rho^{2n+2}, \\ c_{22} &= \sqrt{1-\rho^2-u^2\rho^4}\sum_{n=0}^{\infty}\beta_n\rho^{2n}, \\ c_{32} &= -\sum_{n=0}^{\infty}\frac{\beta_n}{2n+1}\rho^{2n+1}, \\ c_{13} &= -2u\sum_{n=0}^{\infty}\gamma_n\rho^{2n+1}, \\ c_{23} &= -\sqrt{1-\rho^2-u^2\rho^4}\sum_{n=1}^{\infty}2n\gamma_n\rho^{2n-1}, \\ c_{33} &= \sum_{n=0}^{\infty}\gamma_n\rho^{2n}. \end{aligned} \tag{A5}$$

The coefficients $\alpha_n,\beta_n,\gamma_n$ are given by the recursion relations,

$$\begin{aligned} \alpha_1 &= \frac{u}{3},\ \alpha_2 = \frac{2u}{15}, \\ \alpha_{n+1} &= \frac{2n}{2n+3}\alpha_n + u^2\frac{2n-3}{2n+3}\alpha_{n-1},\ n \geqslant 2, \\ \beta_0 &= 1,\ \beta_1 = 0,\ \beta_2 = \frac{4u^2}{3}, \\ \beta_{n+1} &= \frac{2n(2n+2)}{(2n+1)^2}\beta_n + u^2\frac{(2n-3)(2n+2)}{(2n-1)(2n+1)}\beta_{n-1},\ n \geqslant 2, \\ \gamma_0 &= 1,\ \gamma_1 = -1/2, \\ \gamma_{n+1} &= \frac{2n-1}{2n+2}\gamma_n + u^2\frac{2n^2-3n+2}{(2n+1)(n+1)}\gamma_{n-1},\ n \geqslant 1. \end{aligned}$$

[1] Y. Shin, M. Saba, T. A. Pasquini, W. Ketterle, D. E. Pritchard, and A. E. Leanhardt, Phys. Rev. Lett. **92**, 050405 (2004).
[2] M. Albiez, R. Gati, J. Folling, S. Hunsmann, M. Cristiani, and M. K. Oberthaler, Phys. Rev. Lett. **95**, 010402 (2005).
[3] T. Schumm, S. Hofferberth, L. M. Andersson, S. Wildermuth, S. Groth, I. Bar-Joseph, J. Schmiedmayer, and P. Krüger, Nature Phys. **1**, 57 (2005).
[4] J. Esteve, C. Gross, A. Weller, S. Giovanazzi, and M. K. Oberthaler, Nature (London) **455**, 1216 (2008).
[5] P. Böhi, M. F. Riedel, J. Hoffrogge, J. Reichel, T. W. Hänsch, and P. Treutlein, Nature Phys. **5**, 592 (2009).
[6] C. Gross, T. Zibold, E. Nicklas, J. Esteve, and M. K. Oberthaler, Nature (London) **464**, 7292 (2010).
[7] M. F. Riedel, P. Böhi, Y. Li, T. W. Hänsch, A. Sinatra, and P. Treutlein, Nature (London) **464**, 1170 (2010).
[8] P. Bouyer and M. A. Kasevich, Phys. Rev. A **56**, R1083 (1997).
[9] L. Pezze and A. Smerzi, Phys. Rev. Lett. **100**, 073601 (2008); **102**, 100401 (2009).
[10] M. Kitagawa and M. Ueda, Phys. Rev. A **47**, 5138 (1993).
[11] G.-B. Jo, Y. Shin, S. Will, T. A. Pasquini, M. Saba, W. Ketterle, D. E. Pritchard, M. Vengalattore, and M. Prentiss, Phys. Rev. Lett. **98**, 030407 (2007).
[12] J. Grond, U. Hohenester, I. Mazets, and J. Schmiedmyer, New J. Phys. **12**, 065036 (2010).
[13] Y. P. Huang and M. G. Moore, Phys. Rev. Lett. **100**, 250406 (2008).
[14] I. Tikhonenkov, M. G. Moore, and A. Vardi, Phys. Rev. A **82**, 043624 (2010).
[15] A. Imamoglu, M. Lewenstein, and L. You, Phys. Rev. Lett. **78**, 2511 (1997).
[16] Y. Khodorkovsky, G. Kurizki, and A. Vardi, Phys. Rev. Lett. **100**, 220403 (2008); E. Boukobza, M. Chuchem, D. Cohen, and A. Vardi, *ibid.* **102**, 180403 (2009); E. Boukobza, M. G. Moore, D. Cohen, and A. Vardi, *ibid.* **104**, 240402 (2010).
[17] Y. Li, P. Treutlein, J. Reichel, and A. Sinatra, Eur. Phys. J. B **68**, 365 (2009).
[18] J. Chwedeńczuk, L. Pezzé, F. Piazza, and A. Smerzi, Phys. Rev. A **82**, 032104 (2010).
[19] A. Smerzi, S. Fantoni, S. Giovanazzi, and S. R. Shenoy, Phys. Rev. Lett. **79**, 4950 (1997).
[20] A. Vardi and J. R. Anglin, Phys. Rev. Lett. **86**, 568 (2001); I. Tikhonenkov, J. R. Anglin, and A. Vardi, Phys. Rev. A **75**, 013613 (2007); A. Vardi and J. R. Anglin, Phys. Rev. Lett. **75**, 069910(E) (2007).